Acoustically Driven Magnon-Phonon Coupling in a Layered Antiferromagnet

Thomas P. Lyons, Jorge Puebla, Kei Yamamoto, Russell S. Deacon, Yunyoung Hwang, Koji Ishibashi, Sadamichi Maekawa, and Yoshichika Otani

Phys. Rev. Lett. **131**, 196701 — Published 8 November 2023

DOI: 10.1103/PhysRevLett.131.196701

Acoustically driven magnon-phonon coupling in a layered antiferromagnet

Thomas P. Lyons,[1] Jorge Puebla,[1,*] Kei Yamamoto,[2,1] Russell S. Deacon,[3,1] Yunyoung Hwang,[1,4] Koji Ishibashi,[3,1] Sadamichi Maekawa,[1,2,5] and Yoshichika Otani[1,4]

[1]*Center for Emergent Matter Science, RIKEN, Wako-shi, Saitama 351-0198, Japan*
[2]*Advanced Science Research Center, Japan Atomic Energy Agency, Tokai, Ibaraki 319-1195, Japan*
[3]*Advanced Device Laboratory, RIKEN, Wako-shi, Saitama 351-0198, Japan*
[4]*Institute for Solid State Physics, University of Tokyo, Kashiwa, Chiba 277-8581, Japan*
[5]*Kavli Institute for Theoretical Sciences, University of Chinese Academy of Sciences, Beijing 100049, People's Republic of China*

(Dated: September 26, 2023)

Harnessing the causal relationships between mechanical and magnetic properties of van der Waals materials presents a wealth of untapped opportunity for scientific and technological advancement, from precision sensing to novel memories. This can, however, only be exploited if the means exist to efficiently interface with the magnetoelastic interaction. Here, we demonstrate acoustically-driven spin-wave resonance in a crystalline antiferromagnet, chromium trichloride, via surface acoustic wave irradiation. The resulting magnon-phonon coupling is found to depend strongly on sample temperature and external magnetic field orientation, and displays a high sensitivity to extremely weak magnetic anisotropy fields in the few mT range. Our work demonstrates a natural pairing between power-efficient strain-wave technology and the excellent mechanical properties of van der Waals materials, representing a foothold towards widespread future adoption of dynamic magneto-acoustics.

From uncertain beginnings, the technological advantages of antiferromagnets over ferromagnets are now well known, including fast operation, immunity against device crosstalk and stray fields, and amenability to low power control via spin currents or proximitized materials [1, 2]. However, these very same advantageous properties can be a double-edged sword, being partly responsible for a general lack of understanding of antiferromagnets as compared to ferromagnets. The high spin-wave frequencies can be prohibitive for probes based on microwave electronics, while the insensitivity to measurement techniques such as SQUID magnetometry or the magento-optical Kerr effect limit the effectiveness of these popular conventional magnetic probes. A less well-known probe, which has proven itself useful in the study of ferromagnets, relies not on optical or direct magnetic sensing but instead employs the magnetoelastic interaction between spin-waves and acoustic waves [3, 4]. When in contact with a piezoelectric material, the magnetic film can be irradiated with surface acoustic waves (SAWs). Beyond the magnetic film, the transmitted SAWs can be measured, providing information on the magnet's response to external stimuli [3, 5]. Aside from the energy efficient generation, inherently low attenuation, suitability for miniaturization and long distance propagation of SAWs [3, 6, 7], a particular advantage of this technique is that it does not discriminate between ferromagnetic and antiferromagnetic order, and indeed may even be stronger for the latter [8].

SAW technology is relatively mature, having found multiple applications in the microelectronics industry, yet continues to play a key role at the forefront of fundamental research, with recent notable advances including SAW-driven transport of single electrons in gallium arsenide [9], semiconductor interlayer excitons in van der Waals heterobilayers [10], and manipulation of the charge density wave in layered superconductors [11], amongst other advances [7]. Utilizing SAWs as a probe of ferromagnetism has proven highly effective, for instance in understanding the fundamentals of magnetoelasticity and magnetostriction, or more recently in revealing the various mechanisms of SAW nonreciprocity [3, 5, 12–17]. Such works have laid the foundations for the active field of SAW-spintronics, in which dynamically applied strain can modulate magnetic properties [6, 18]. This technique is mature for ferromagnets, and has recently been proven effective for multiferroics [19] and synthetic antiferromagnets [14, 20], but a demonstration of SAW-driven magnon-phonon coupling in a crystalline antiferromagnet remains elusive.

Here, we utilize SAWs to drive spin-wave resonance in a layered crystalline antiferromagnet, chromium trichloride ($CrCl_3$), a material characterized by layers of alternating magnetization weakly bound by van der Waals attraction [21, 22]. The antiferromagnetic order occurs only between adjacent monolayers rather than within them, giving rise to relatively weak interlayer exchange and associated lower frequency range of spin excitations in $CrCl_3$ as compared to conventional antiferromagnets [21, 23]. The combination of easy flake transfer onto arbitrary substrates, with sub-10 GHz spin excitations, is advantageous for integration of $CrCl_3$ into SAW devices, where antiferromagnetic magnetoelasticity can be probed directly. After first demonstrating acoustic antiferromagnetic resonance, we proceed to study the influence of temperature and angle of applied external magnetic field on the magnon-phonon coupling. The sets of experimental data are analyzed by extending the established the-

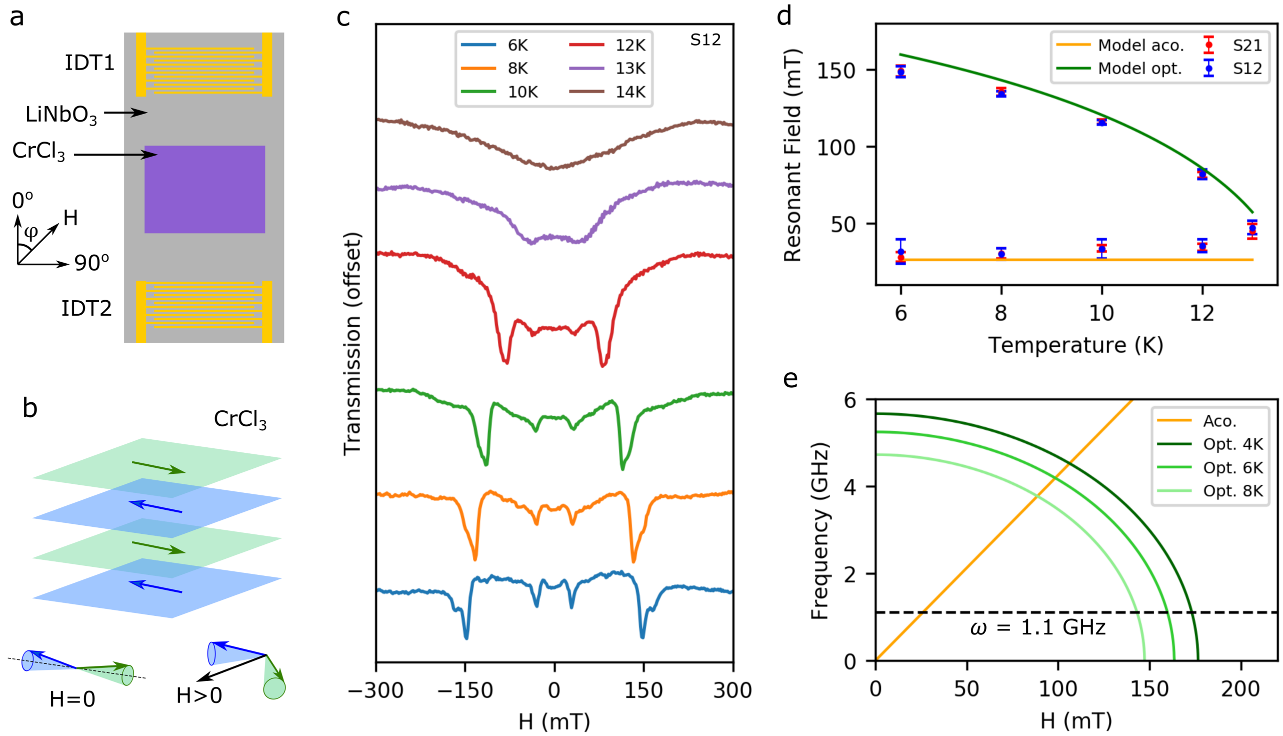

FIG. 1. **Magnon-phonon coupling in layered $CrCl_3$.** (a) Schematic of the devices used in this work. See text for description. (b) $CrCl_3$ consists of stacked ferromagnetic layers of alternating in-plane magnetization, represented by two spin sublattices (green and blue arrows). In the absence of an external magnetic field, the sublattice magnetizations point away from each other, while an applied field causes them to cant. In-phase and out-of-phase precession of the sublattice magnetizations are associated with acoustic and optical magnon modes, respectively. (c) SAW transmission signal from IDT2 to IDT1 (termed S12) through $CrCl_3$ in Sample 1 as a function of applied magnetic field strength at an angle $\phi = 45°$, at various sample temperatures. (d) Extracted resonance field strengths for the acoustic and optical magnon modes at various Sample 1 temperatures. Overlaid curves are calculated from the model described in the text. (e) Calculated frequency dependence of the acoustic and optical magnon modes as a function of applied magnetic field, at $T = 4, 6$ and 8 K.

oretical model for SAW-spin wave coupling in ferromagnetic films [4, 5]. Combined with a mean-field calculation of the temperature dependence, our model reproduces the observed features well, confirming the amenability of SAWs as a powerful probe to elucidate the dynamics of van der Waals magnets, especially given their excellent plasticity [24]. Considering also that acoustic magnetic resonance generates spin currents, which have been shown to travel over long distances in antiferromagnets, our results offer an alternative route towards novel spintronic devices with layered crystals [25–28].

Two devices are studied in this work. They each consist of lithium niobate ($LiNbO_3$) substrates with aluminium interdigital transducers (IDTs) either side of a $CrCl_3$ flake (Fig. 1a). Each IDT, 1 or 2, can generate SAWs at 1.1 GHz and wavelength 3.2 μm, which subsequently propagate along the surface of the $LiNbO_3$, interact with the $CrCl_3$ flake, and then reach the other IDT where they are detected. By measuring SAW transmission in this way, any absorption of acoustic energy by the antiferromagnet can be detected (see methods). Sample 1 is quasi-bulk, at ~ 4 μm thick, while Sample 2 is much thinner at ~ 120 nm [29].

Below the Néel temperature of ~ 14 K, layered $CrCl_3$ is composed of stacked ferromagnetic layers ordered antiferromagnetically [21, 22]. Alternate layers belong to one of two spin sublattices oriented collinearly in the layer plane, owing to easy plane anisotropy of strength $\sim$ 250 mT (Fig. 1b) [21]. Two magnon modes arise from in-phase or out-of-phase precession of the two sublattice macrospins, described as acoustic and optical modes, respectively [23]. In our experiments we apply an external magnetic field perpendicular to the crystal c-axis, inducing the two spin sublattice magentizations to cant towards the applied field direction (Fig. 1b). Such noncollinear canting modifies their precession frequency, thereby bringing the magnon modes into resonance with the acoustic wave.

We first apply an external magnetic field at an angle $\phi = 45°$ to the SAW propagation direction in Sample 1, and measure the amplitude of the SAW transmission. The result is shown in Fig. 1c, where clear transmission

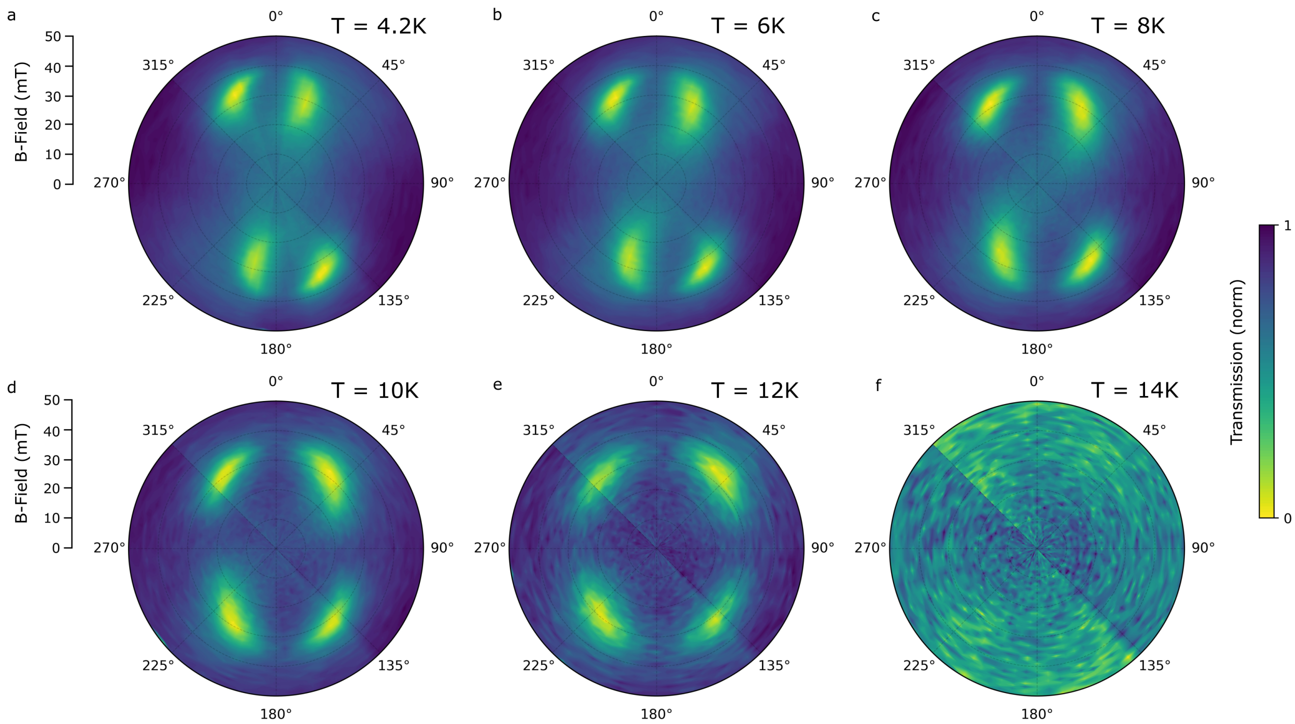

FIG. 2. **Acoustic magnon mode dependence on external field angle and temperature** (a-f) Polar plots of SAW absorption by the acoustic magnon mode in Sample 2, at various sample temperatures, as a function of applied external magnetic field orientation in the sample plane. Asymmetry at lower temperatures arises due to very weak uniaxial anisotropy ~ 2 mT. Upon heating, the expected symmetric response of the magnetoelastic interaction is recovered. Absorption disappears at $T = 14$ K, close to the Néel temperature.

dips can be seen arising from absorption of SAWs by magnons. At $T = 6$ K, absorption is observed at approximately 30 and 150 mT, attributed to the acoustic and optical modes, respectively. Examples of other external field orientations can be seen in the SI. At the lowest temperatures in Fig. 1c, the optical mode can be seen to form a doublet fine structure. At present we ascribe this to emergence of non-degenerate bulk and surface magnon modes, however, this is the subject of ongoing investigations.

Upon heating the sample, the optical mode absorption shifts to lower resonance field strengths while the acoustic mode stays largely insensitive to temperature (Fig. 1d). At $T = 13$ K, the two modes are no longer resolved, and at $T = 14$ K, close to the Néel temperature [21], they have disappeared. We note that measurements at $T > 14$ K did not yield any clear SAW absorption. While ferromagnetic order has been reported in $CrCl_3$ between $T = 14$ and 17 K [21], this order is short range and therefore does not seem to offer enough collective strength over the SAW wavelength of 3.2 μm to effectively observe coupling behavior.

The observed temperature dependence of the resonance field can be modelled by combining a simple mean-field theory with the known formulae for spin wave resonance in easy-plane antiferromagnets [23]

$$H_{\mathrm{res}} = \begin{cases} \sqrt{2H_E/(2H_E + M_s)}\,\omega/\gamma & \text{acoustic} \\ \sqrt{4H_E^2 - 2H_E\omega^2/(M_s\gamma^2)} & \text{optical} \end{cases} \tag{1}$$

Here H_E is the interlayer exchange field, M_s is the saturation magnetization, ω is the SAW frequency, and $\gamma/2\pi = 28$ GHz/T is the gyromagnetic ratio respectively. We solve the molecular field equation self-consistently in the macrospin limit $S \to \infty$ to obtain $M_s(T)$. This approximation also implies $H_E(T) \propto M_s(T)$, which predicts the optical mode resonance field tends towards zero as the Néel temperature is approached while the acoustic mode remains unchanged. The calculated temperature dependence is plotted in Fig. 1d and agrees well with the experimental data. The small increase of the observed acoustic mode resonance field towards higher temperature [30] points to breakdown of the mean-field approximation near the phase transition. The same model can be used to calculate the effective magnon frequency evolution as a function of applied magnetic field strength, as shown in Fig. 1e.

We now consider the coupling between SAWs and the acoustic magnon mode in greater detail. Figure 2 shows absorption by the acoustic mode as a function of external

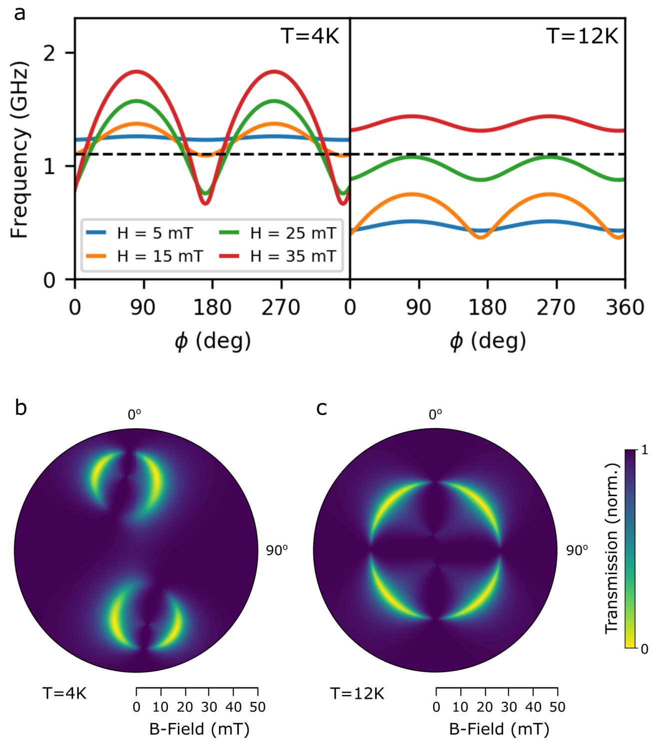

FIG. 3. **Theoretical model for acoustic mode** (a) Calculated acoustic mode frequency dependence on external magnetic field orientation ϕ. (b, c) Simulated polar plots of SAW absorption by the acoustic magnon as a function of external magnetic field orientation, using parameters for Sample 2. The striking difference in response is largely attributed to a change in anisotropy of only ~ 1 mT.

magnetic field orientation in the plane of Sample 2, where the vertical axis (0° - 180° line) is the SAW propagation axis. At $T = 4.2$ K, we observe four lobes of strong absorption, seen only when the external magnetic field is applied at angles smaller than 45° to the SAW propagation axis. As the temperature is increased to $T = 12$ K, they migrate to new positions which are more rotationally symmetric. By $T = 14$ K, close to the Néel temperature, the absorption has disappeared, in agreement with Sample 1.

To fully understand the results in Fig. 2, we must consider the interplay between antiferromagnetic resonance and magnon-SAW coupling. Each has its own dependence on external magnetic field orientation, with the latter defining the window through which we can observe the former. Firstly we focus on the magnetic response of $CrCl_3$ itself. Close inspection of Fig. 2a reveals that not only the magnitude of absorption but also the resonance field depends strongly on the magnetic field angle ϕ at $T = 4.2$ K, indicating the presence of magnetic uniaxial anisotropy. To reproduce this observation, we calculate the acoustic mode resonance frequency as a function of ϕ computed for a model that includes an in-plane uniaxial anisotropy field $\mu_0 H_u \approx 2.1$ mT, oriented approximately along the line 171° - 351°. Although this anisotropy is itself very weak, it induces a sizable zero-field magnon frequency gap of $\gamma\mu_0\sqrt{2H_u(2H_E + M_s + H_u)} \sim 1.2$ GHz, above the SAW frequency of 1.1 GHz. As can be seen at $T = 4$ K in Fig. 3a, for $30° \lesssim \phi \lesssim 130°$ and $210° \lesssim \phi \lesssim 310°$, the frequency monotonically increases as H increases so that the acoustic magnon never becomes resonant with the SAWs. Only in the remaining angular ranges are acoustic spin-wave resonances observable, which correspond to the lobes in Fig. 2a.

According to the well-known formula $H_u(T) \propto M_s(T)^2$ [31], the uniaxial anisotropy tends to zero as T increases towards the Néel point. We find it reduces to ≈ 0.6 mT at $T = 12$ K, lowering the zero-field magnon frequency below the SAW frequency, and thereby allowing acoustic magnon resonance at 1.1 GHz for all angles at around $25 - 30$ mT (Fig. 3a). While uniaxial anisotropy of ~ 1 mT has been observed before in $CrCl_3$ [32], the origin remains ambiguous. Here, we tentatively ascribe it to negative thermal expansion in $CrCl_3$, in which the a-axis lattice parameter gradually increases upon cooling the crystal below $T = 50$ K, owing to magnon induced expansion of the lattice [33, 34]. Our results hint at the applicability of SAWs to further investigate this poorly understood effect, or moreover exploit it for highly sensitive static strain or force sensing applications.

To complete the picture, we now consider the magnon-SAW coupling dependence on external field orientation, which has proven the key to accessing various parameters in ferromagnetic materials [5]. Given that, unlike ferromagnets, the antiferromagnetic sublattice magnetizations do not simply align with the external field, we model the magnetoelastic coupling in $CrCl_3$ by a free energy density $F_{\rm me} = b\epsilon_{ab}(n_a^A n_b^A + n_a^B n_b^B) + 2c\epsilon_{ab} n_a^A n_b^B$. Here ϵ_{ab} is the strain tensor, n_a^A, n_a^B are components of the normalized sublattice magnetization vectors, and Einstein's summation convention is assumed. b is an intrasublattice magnetoelastic coefficient, a direct generalization of the ferromagnetic magnetoelasticity. c is an intersublattice coefficient, unique to antiferromagnets, which was studied in literature [35]. Let ϕ_A, ϕ_B be the angles between the SAW propagation direction and the respective sublattice magnetizations. The corresponding magnon-SAW couplings g_A, g_B exhibit the following angle dependence (see SI):

$$g_A \propto b \sin\phi_A \cos\phi_A + c \sin\phi_A \cos\phi_B, \tag{2}$$

$$g_B \propto b \sin\phi_B \cos\phi_B + c \sin\phi_B \cos\phi_A. \tag{3}$$

The acoustic and optical modes see $g_A \pm g_B$ respectively, reflecting the phase relations between the two sublattices. For acoustic mode resonance, H is small so that $\phi_B \approx \phi_A + \pi \approx \phi \pm \pi/2$, yielding $g_A + g_B \propto \sin 2\phi$. This acoustic magnon-SAW coupling filters the nominally observable resonance frequencies shown in Fig. 3a to give the cumulative responses shown in Fig. 3b, c, in which vanishing absorption can be seen at $\phi = 0°, 90°, 180°, 270°$. The agreement with Fig. 2a, e is satisfactory.

Next, we consider optical magnon-phonon coupling. Figures. 4a, b show the optical mode absorption in Sample 2, seen to some extent at every angle of applied field. This isotropic behaviour, in stark contrast to that displayed by the acoustic mode, arises because the two canted spin sublattices adopt an almost parallel configuration at the relatively high field strength needed to reach resonance, i.e. $\phi_A \approx \phi + \delta, \phi_B \approx \phi - \delta, |\delta| \ll \pi$. Equations (2) and (3) therefore yield $g_A - g_B \propto (b \cos 2\phi + c) \sin 2\delta$. We note that the intra-sublattice coupling b alone gives a vanishing absorption at $\phi = 45°$, inconsistent with both Sample 1 (Fig. 1c) and Sample 2 (Fig. 4a, b). Hence we take $b = 0, c \sim 10^6$ J/m^3 with the aforementioned temperature dependent H_E, M_s, H_u to generate Figs. 4c, d, which show the simulated optical mode absorption at $T = 4$ K and 13 K, respectively. The agreement with experiment is satisfactory at $T = 4.2$ K, and reasonable at $T = 13$ K, given the simplifications to the model (such as an absence of broadening/disorder) and the expected breakdown of the mean-field approximation close to the phase transition.

In conclusion, we demonstrate GHz-range SAW-driven magnon-phonon coupling in a crystalline antiferromagnet, complimenting the existing studies of spin wave spectra for the same material by neutron scattering, in which evidence of Dirac magnons was reported for high SAW frequencies [33, 36]. Our demonstration, addressing the less well-studied lower frequency range, paves the way towards acoustically driven spintronic devices based on designer van der Waals heterostructures, which may combine antiferromagnetic, semiconducting, metallic and insulating layers to realise diverse outcomes in spin conversion [28, 37]. Moreover, it has been proposed that monolayer $CrCl_3$ exhibits true 2D XY-ferromagnetism, allowing study of the Berezinskii–Kosterlitz–Thouless phase transition [38], and predicted to play host to topological spin textures [39]. Creation and manipulation of such excitations by SAWs is a tantalising prospect, as has been recently achieved in conventional ferromagnetic systems [40].

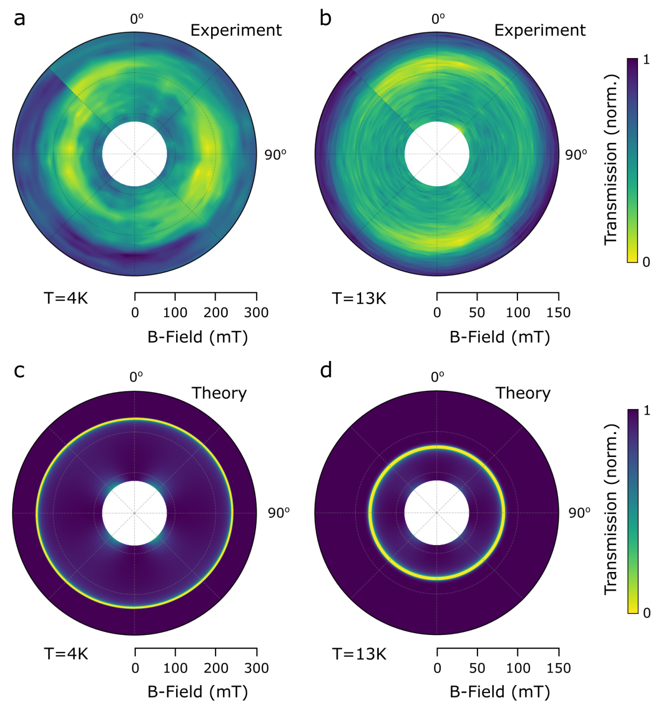

FIG. 4. **Optical magnon mode dependence on external field angle and temperature** (a, b) Experimental and (c, d) simulated polar plots of SAW absorption by the optical mode in Sample 2 as a function of external magnetic field orientation at $T = 4.2$ K and 13 K. Line cuts of this data can be found in [29].

ACKNOWLEDGEMENTS

The authors would like to thank Joseph Barker, Olena Gomonay, Hidekazu Kurebayashi, Philipp Pirro, and Sean Stansill for helpful comments. TPL acknowledges support from the JSPS postdoctoral fellowships for research in Japan scheme, and KY from JST PRESTO Grant No. JPMJPR20LB, Japan and JSPS KAKENHI (No. 21K13886). JP is financially supported by Grants-in-Aid for Scientific Research (S) (No. 19H05629) and JSPS KAKENHI (20H01865), from MEXT, Japan. RSD is supported by Grants-in-Aid for Scientific Research (S) (No. 19H05610), from MEXT, Japan. Y.H. is supported by the RIKEN Junior Research Associate Program. SM is financially supported by JST CREST Grant (No.JPMJCR19J4, No.JPMJCR1874 and No.JPMJCR20C1) and JSPS KAKENH (No.17H02927 and No.20H10865) from MEXT, Japan. YO is is financially supported by Grants-in-Aid for Scientific Research (S) (No. 19H05629).

AUTHOR CONTRIBUTIONS

T. P. L., J. P. and R. S. D. performed experiments. T. P. L., J. P. and Y. H. fabricated samples. All authors contributed to data interpretation and analysis. K. Y. and S. M. developed the theoretical model. T. P. L. and K. Y. wrote the paper. J. P. and Y. O. initiated and supervised the project.

* jorgeluis.pueblanunez@riken.jp

[1] T. Jungwirth, X. Marti, P. Wadley, and J. Wunderlich, Nature Nanotechnology **11**, 231 (2016).

[2] S. Fukami, V. O. Lorenz, and O. Gomonay, Journal of Applied Physics **128** (2020), 10.1063/5.0023614.

[3] J. Puebla, M. Xu, B. Rana, K. Yamamoto, S. Maekawa, and Y. Otani, Journal of Physics D: Applied Physics **53** (2020), 10.1088/1361-6463/ab7efe.

[4] K. Yamamoto, M. Xu, J. Puebla, Y. Otani, and S. Maekawa, Journal of Magnetism and Magnetic Materials **545** (2022), 10.1016/j.jmmm.2021.168672.

[5] M. Xu, K. Yamamoto, J. Puebla, K. Baumgaertl, B. Rana, K. Miura, H. Takahashi, D. Grundler, S. Maekawa, and Y. Otani, Sci. Adv **6** (2020), 10.1126/sciadv.abb1724.

[6] L. Dreher, M. Weiler, M. Pernpeintner, H. Huebl, R. Gross, M. S. Brandt, and S. T. Goennenwein, Physical Review B **86** (2012), 10.1103/PhysRevB.86.134415.

[7] X.-C. Nie, X. Wu, Y. Wang, S. Ban, Z. Lei, J. Yi, Y. Liu, and Y. Liu, Nanoscale Horizons (2022), 10.1039/d2nh00458e.

[8] T. Yamada, S. Saito, and Y. Shimomura, Journal of the Physical Society of Japan **21**, 672 (1966).

[9] J. Wang, S. Ota, H. Edlbauer, B. Jadot, P. A. Mortemousque, A. Richard, Y. Okazaki, S. Nakamura, A. Ludwig, A. D. Wieck, M. Urdampilleta, T. Meunier, T. Kodera, N. H. Kaneko, S. Takada, and C. Bäuerle, Physical Review X **12** (2022), 10.1103/PhysRevX.12.031035.

[10] R. Peng, A. Ripin, Y. Ye, J. Zhu, C. Wu, S. Lee, H. Li, T. Taniguchi, K. Watanabe, T. Cao, X. Xu, and M. Li, Nature Communications **13** (2022), 10.1038/s41467-022-29042-9.

[11] M. Yokoi, S. Fujiwara, T. Kawamura, T. Arakawa, K. Aoyama, H. Fukuyama, K. Kobayashi, and Y. Niimi, Sci. Adv **6** (2020), 10.1126/sciadv.aba1377.

[12] R. Sasaki, Y. Nii, Y. Iguchi, and Y. Onose, Phys. Rev. B **95**, 020407 (2017).

[13] A. Hernández-Mínguez, F. Macià, J. M. Hernàndez, J. Herfort, and P. V. Santos, Phys. Rev. Appl. **13**, 044018 (2020).

[14] R. Verba, V. Tiberkevich, and A. Slavin, Physical Review Applied **12** (2019), 10.1103/PhysRevApplied.12.054061.

[15] M. Küß, M. Heigl, L. Flacke, A. Hörner, M. Weiler, M. Albrecht, and A. Wixforth, Phys. Rev. Lett. **125**, 217203 (2020).

[16] M. Küß, M. Heigl, L. Flacke, A. Hörner, M. Weiler, A. Wixforth, and M. Albrecht, Phys. Rev. Appl. **15**, 034060 (2021).

[17] P. J. Shah, D. A. Bas, I. Lisenkov, A. Matyushov, N. X. Sun, and M. R. Page, Science Advances **6**, eabc5648 (2020).

[18] J. Puebla, Y. Hwang, S. Maekawa, and Y. Otani, Applied Physics Letters **120** (2022), 10.1063/5.0093654.

[19] R. Sasaki, Y. Nii, and Y. Onose, Physical Review B **99** (2019), 10.1103/PhysRevB.99.014418.

[20] H. Matsumoto, T. Kawada, M. Ishibashi, M. Kawaguchi, and M. Hayashi, Applied Physics Express **15** (2022), 10.35848/1882-0786/ac6da1.

[21] M. A. McGuire, G. Clark, S. Kc, W. M. Chance, G. E. Jellison, V. R. Cooper, X. Xu, and B. C. Sales, Physical Review Materials **1** (2017), 10.1103/PhysRevMaterials.1.014001.

[22] A. Narath and H. L. Davis, Physical Review **137** (1965), 10.1103/PhysRev.137.A163.

[23] D. Macneill, J. T. Hou, D. R. Klein, P. Zhang, P. Jarillo-Herrero, and L. Liu, Physical Review Letters **123** (2019), 10.1103/PhysRevLett.123.047204.

[24] F. Cantos-Prieto, A. Falin, M. Alliati, D. Qian, R. Zhang, T. Tao, M. R. Barnett, E. J. Santos, L. H. Li, and E. Navarro-Moratalla, Nano Letters **21**, 3379 (2021).

[25] D. D. Awschalom, C. R. Du, R. He, F. J. Heremans, A. Hoffmann, J. Hou, H. Kurebayashi, Y. Li, L. Liu, V. Novosad, *et al.*, IEEE Transactions on Quantum Engineering **2**, 1 (2021).

[26] R. Lebrun, A. Ross, S. A. Bender, A. Qaiumzadeh, L. Baldrati, J. Cramer, A. Brataas, R. A. Duine, and M. Kläui, Nature **561**, 222 (2018).

[27] K. S. Burch, D. Mandrus, and J. G. Park, Nature **563**, 47 (2018).

[28] T. S. Ghiasi, A. A. Kaverzin, A. H. Dismukes, D. K. de Wal, X. Roy, and B. J. van Wees, Nature Nanotechnology **16**, 788 (2021).

[29] See supplemental material in XXX.XXX. for further information on the theoretical model (note 1), methods and sample details, which includes Refs.[4, 14, 21, 23, 31, 41, 42].

[30] J. Zeisner, K. Mehlawat, A. Alfonsov, M. Roslova, A. Doert, T.and Isaeva, B. Büchner, and V. Kataev, Physical Review Materials **4**, 064406 (2020).

[31] H. B. Callen and E. Callen, Journal of Physics and Chemistry of Solids **27**, 1271 (1966).

[32] B. Kuhlow, physica status solidi (a) **72**, 161 (1982).

[33] J. A. Schneeloch, Y. Tao, Y. Cheng, L. Daemen, G. Xu, Q. Zhang, and D. Louca, npj Quantum Materials **7** (2022), 10.1038/s41535-022-00473-3.

[34] S. Liu, M. Q. Long, and Y. P. Wang, Applied Physics Letters **120** (2022), 10.1063/5.0084070.

[35] A. S. Borovik-Romanov and E. G. Rudashevskii, Journal of Experimental and Theoretical Physics **20**, 1407 (1965).

[36] L. Chen, M. B. Stone, A. I. Kolesnikov, B. Winn, W. Shon, P. Dai, and J.-H. Chung, 2D Materials **9** (2022), 10.1088/2053-1583/ac2e7a.

[37] Y. Otani, M. Shiraishi, A. Oiwa, E. Saitoh, and S. Murakami, Nature Physics **13**, 829 (2017).

[38] J. M. Kosterlitz and D. J. Thouless, Journal of Physics C: Solid State Physics **6**, 1181 (1973).

[39] A. Bedoya-Pinto, J.-R. Ji, A. K. Pandeya, P. Gargiani, M. Valvidares, P. Sessi, J. M. Taylor, F. Radu, K. Chang, and S. S. P. Parkin, Science **374**, 616 (2021).

[40] T. Yokouchi, S. Sugimoto, B. Rana, S. Seki, N. Ogawa, S. Kasai, and Y. Otani, Nature Nanotechnology **15**, 361 (2020).

[41] J. L. Rose, *Ulstrasonic Waves in Solid Media* (Cambridge University Press, Cambridge, 1999).

[42] K. Yamamoto, W. Yu, T. Yu, J. Puebla, M. Xu, S. Maekawa, and G. Bauer, Journal of the Physical Society of Japan **89**, 113702 (2020).